Supplementary Information: Adsorption Dynamics of CVD Graphene Investigated by a Contactless Microwave Method

NCG Black[1,2], I Rungger[1], B Li[2], SA Maier[2], LF Cohen[2], J Gallop[1] and L Hao[1]

[1] National Physical Laboratory, Hampton Road, Teddington, TW11 0LW, UK
[2] Department of Physics, Imperial College London, London SW7 2AZ, UK

S1 The Microwave Method

Figure S1 depicts a schematic of the experimental apparatus used to measure the linewidth perturbation of the graphene coupled dielectric resonator.

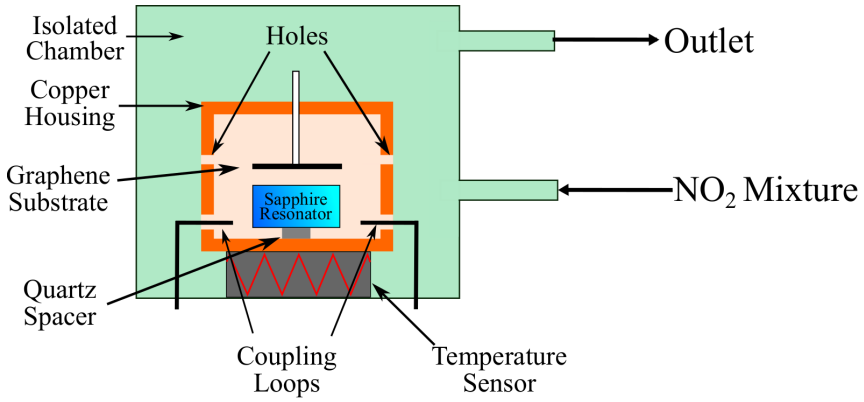

Figure S1: Schematic of the graphene coupled to the microwave dielectric resonator cavity.

By measuring the perturbation of the resonant mode the dielectric cavity due to the presence of a graphene sample, the graphene sheet resistivity can be calculated. The technique relies on a number of crucial factors. First, that graphene is atomically thin. Therefore, the presence of graphene does not significantly perturb the total field distribution around the resonator and its permittivity is close to unity. Secondly, the presence of graphene and substrate will shift the resonant frequency position and linewidth of the resonator. Consequently, the sheet resistance (R_s) of graphene can be calculated by measuring the perturbation of the resonance frequency and linewidth of a dielectric cavity in the presence of a graphene coated substrate as follows:

$$R_s = \frac{\Delta f_s}{\pi f_0 \epsilon_0 (\Delta w_g - \Delta w_s)(\epsilon' - 1) t_s} \tag{S1}$$

Here Δf_s is the frequency shift of the bare substrate, f_0 is the unperturbed resonant frequency of the cavity, Δw_g and Δw_s are the changes of linewidth in the presence of the graphene coated

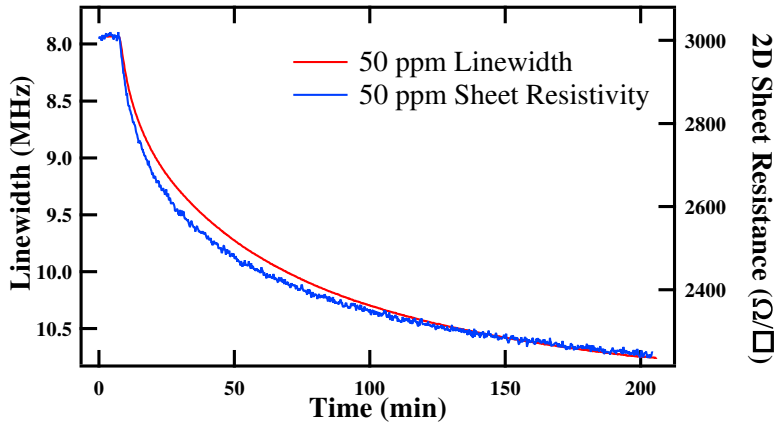

Figure S2: Comparison of the linewidth and calculated 2D sheet resistivity of graphene during 50 ppm NO_2 exposure.

substrate and the bare substrate respectively, ϵ_0 is the permittivity of free space, ϵ' is the real permittivity of the substrate and t_s is the substrate thickness. The full derivation of equation (S1) can be found in reference [1]. Therefore, by placing the cavity in an isolated chamber where the atmosphere can be controlled, the doping level of graphene can be ascertained by following the change of linewidth; which is inversely proportional to the 2D sheet resistivity.

S2 Sample Fabrication

CVD graphene/Cu (purchased from Graphenea) was transferred onto a pure silicon substrate, (purchased from CrysTec GmbH) using a modified wet transfer procedure [2, 3, 4, 5, 6]. To summarise the procedure, first the graphene/Cu stack was protected with a thin layer of (polymethyl methacrylate) PMMA A4 495 by spin coating. The PMMA film was approximately 200 nm thick. The copper was then etched by floating the stack on a 0.1 M solution of ammonium persulfate and leaving it over night. The resulting PMMA/graphene stack was rinsed using deionised water to remove any ion residuals. The stack was 'scooped' out of the deionised water using the target high resistance silicon substrate. After drying, the sample was annealed for 30 minutes at 180°C to facilitate polymer reflux and encourage graphene adhesion to the substrate. Finally the PMMA was removed in acetone and rinsed in isopropyl alcohol (IPA). Once dry the graphene sample was annealed again at 180°C for 10 minutes to further improve substrate adhesion.

S3 Sensor Recovery and Reproducibility

The conductivity of graphene is directly dependent to the number of occupied adsorption sites on the 2D surface facilitating charge transfer. Since the linewidth is inveresely proportional to the graphene sheet resistivity, a consistent initial linewidth value was chosen for each concentration measurement. In other words, the sensor response is normalized by this initial linewidth. The initial linewidth needs to be equal for all considered NO_2 concentrations, in order to have consistent numbers. We use the value of 8.7 MHz.

To illustrate this, Figure S3 compares five adsorption measurements, three exposed to 0.3 ppm of NO_2 and two exposed to 3 ppm. All measurements start at a different initial linewidth value

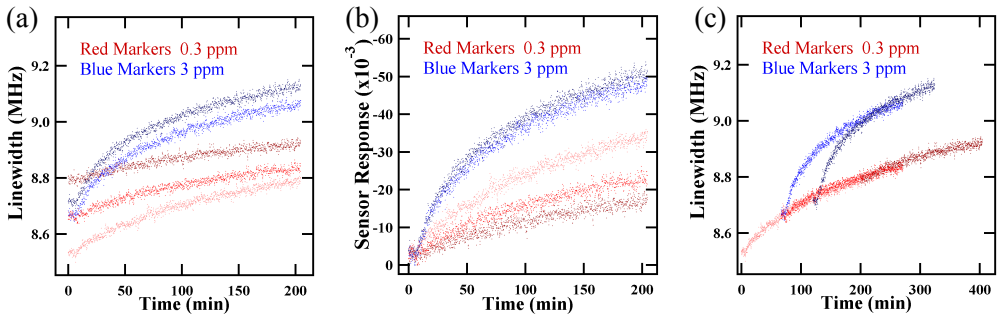

Figure S3: (a) Change in linewidth during gas exposure when starting at different initial linewidth values, and (b) the resulting sensor response curves. (c) Offsetting the linewidth data along the x-axis clearly shows that the sensor responses are dependent on occupancy of the graphene surface.

(Figure S3a). Clearly, the sensor responses are not comparable as shown in Figure S3b since the initial doped state of the graphene is inconsistent. Interestingly, when offsetting the measurements, as shown in Figure S3c, it is clear that there is an overarching response trend dependent on the gas concentrations. The data was offset such that the linewidth values of the"slow" phase overlapped. This is easiest to see in the 0.3 ppm data as the concentration is low enough that only the adsorption sites with lowest adsorption energy barrier are occupied. The 3 ppm concentration measurement show two distinct responses, a rapid initial adsorption followed by a slower response. The initial slopes of the 3 ppm curves match very well (Figure S3b) and when the curves are offset (Figure S3c, the higher linewidth values overlap, the slow adsorption region. This indicates an overall sensor response shape that is dependent upon only the degree of doping of the sample i.e. how many gas molecules are adsorbed and donating a charge carrier. This confirms the importance of sensor responses having comparable initial linewidths.

In order to have comparable initial linewidths, the sample was recovered by allowing NO_2 to desorb and diffuse out of the system. To promote NO_2 desorption air was flowed through the system. Figure S4 follows the recovery of a graphene sensor. In region 1 the sensor is exposed to 3 ppm NO_2 gas where the increase in linewidth is due to NO_2 adsorption. In region 2 the NO_2/ synthetic air mixture inlet valve is closed; leaving the gas to diffuse through the system and exit through the outlet valve. In region 3, air is flowed through the system enhancing the removal of NO_2 through the outlet and encouraging the desorption of NO_2 from the graphene surface. The desorption time scale is much longer than the adsorption timescale. In this work, to ensure graphene integrity, the desorption of NO_2 was not enhanced by increasing the temperature, exposure to UV light or pumping down the system to vacuum.

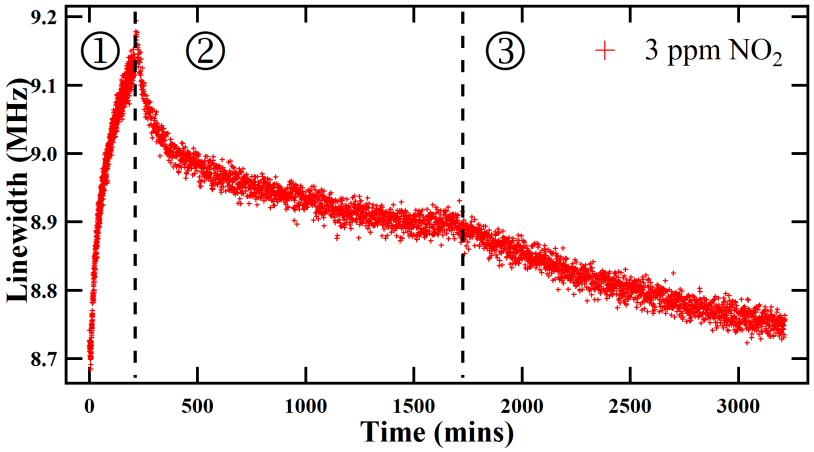

Figure S4: The full sensor response and recovery for 3 ppm NO_2. In region 1 NO_2 is flowed through the sensor. In region 2, the valves are closed and the samples is left to desorb NO_2. In region 3 air is then flowed into the system to promote further desorption of NO_2.

S4 Empirical Data Fitting

Aside from the low concentration curve at 0.3 ppm, where a single exponential expression is sufficient to fit the data (Figure S5a), a minimum of two exponentials were required to fit all other response curves (Figure S5b). In principle it was found that a stretched exponential expression, $S_t = S_e - K\exp\{-t/\tau_s\}^{\beta}$, also known as a Kohlrausch function, can also be used to approximately fit the sensor response (Figure S5c). Here S_t is the linewidth at time t, S_e is the value at equilibrium, K is an amplitude coefficient, τ_s is the time constant associated with the exponential term and β is an exponent such that $0<\beta\leq 1$. The drawback of this function however is that for $\beta < 1$, which is the regime required to the experimental data, it has an unphysical infinite slope at $t = 0$, while the experimental data always starts with a finite slope. The two exponentials were therefore used instead for the fitting, as they avoid this unphysical behavior, and also allow for more flexibility in the functional form.

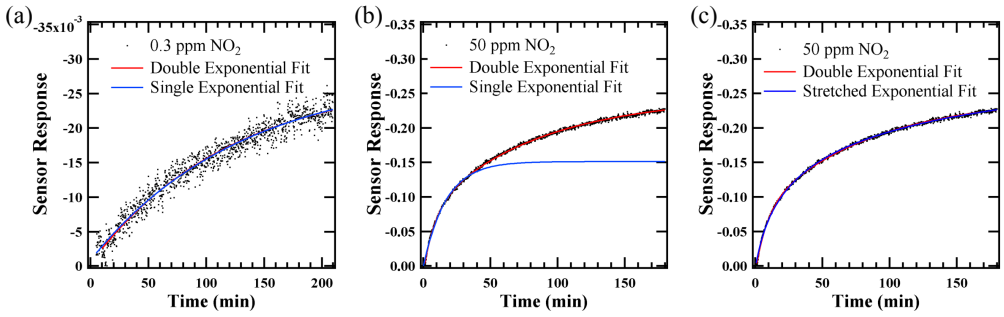

Figure S5: (a) Fitting the 0.3 ppm sensor to both a single and a double exponential expression. (b) The 50 ppm sensor response cannot be fitted with both a single exponential and a double exponential expression for comparison purposes. (c) The stretched and the double exponential expressions fit the 50 ppm data equally well.

S5 KPFM Analysis

Full Kelvin Peak Force Microscopy (KPFM) data for a monolayer only graphene region and a region of both multi and monolayer graphene regions, Figure S6 and Figure S7 respectively. In both cases the atomic force microscopy (AFM) images show a continuous graphene film transferred onto the substrate. From the KPFM and tip adhesion maps (Figure S7b and c), the small multilayer region island is clearly visible. The corresponding histogram (Figure S7d) is the convolution of two normal distributions. This is due to a charge screening effect preventing the substrate from influencing the top graphene film in the multilayer region as strongly as the monolayer region [7]. Although there are two distinct regions associated with monolayer and multilayer graphene, it is clear that the overall distribution of energy states is still continuous, although slightly skewed from the normal distribution.

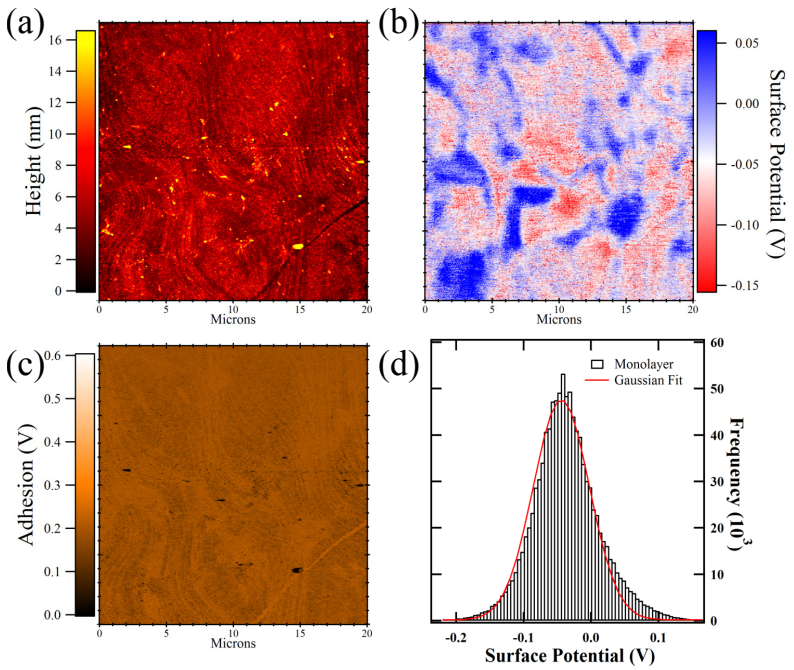

Figure S6: (a)AFM, (b) KFM, (c) tip adhesion, and (d) histogram of total KFM map of monolayer region on the graphene sample.

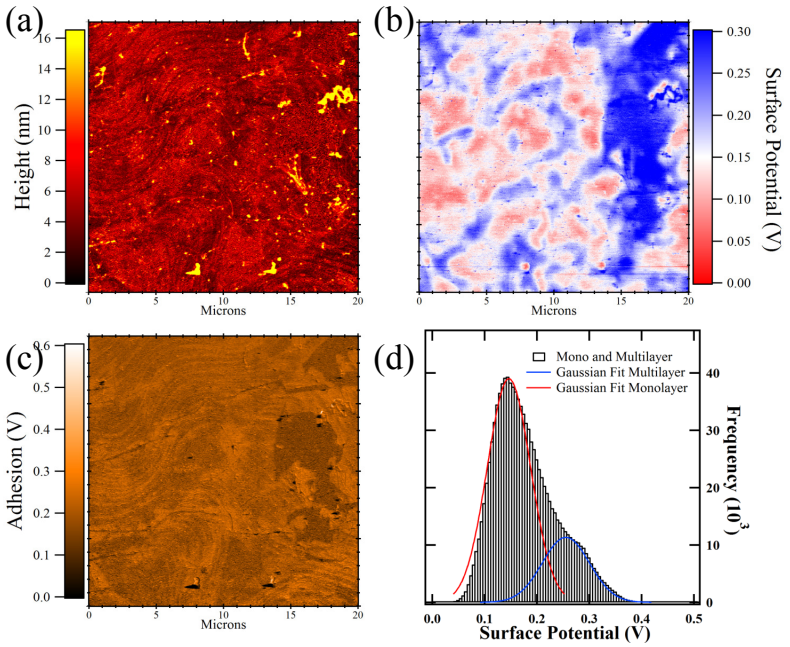

Figure S7: (a)AFM, (b) KFM, (c) tip adhesion, and (d) histogram of total KFM map of monolayer and multilayer regions on the graphene sample.

S6 Raman Maps

Figure S8 shows the local variation of the Raman properties of graphene. Raman maps of the D, G and 2D peak show the peak intensity (figure S8a-c), full width and half maximum (figure S8e-g) and peak position (figure S8h-j) variation over a 10 x 20 μm area. The large quantity of black pixels present in the D maps correspond to unsuccessful fitting of the D peak due to a lack of spectral intensity. Consequently, since the D peak is nominally present at the edges, boundaries or defected regions of graphene, the inability for the curve fit procedure to distinguish a Raman peak from the baseline noise is indicative of a low defect concentration. Histograms comparing the intensity, position and full width at half maximum of the D, G and 2D Raman peaks are shown in figures S8j-l respectively. As part of the peak fit procedure, if the peak fit fails the value is set to zero which is clearly shown in the histogram data.

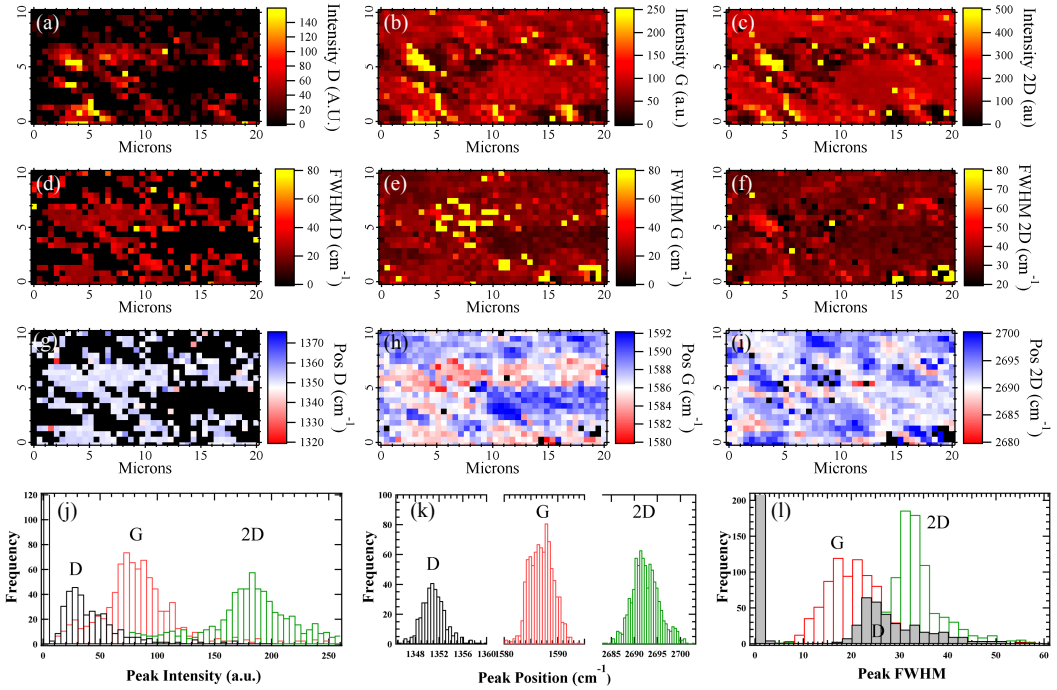

Figure S8: Raman maps of graphene the D, G and 2D Raman peaks with respect to peak (a-c) intensity, (d-f) full width at half maximum and (g-i) position. Corresponding histograms (j-l) compare the D, G and 2D Raman peak intensity, full width half maximum and position data. The D peak histogram data of (l) was shaded black as a guide for the eyes. Raman peaks that were unsuccessfully fitted were set to zero. Note that the D peak histogram data has 1213 counts in the zero value bin which is not shown in the graph.

S7 Theoretical Model

In this section we present a detailed description of the theoretical model. We start from a general model for the adsorption rate of NO_2 molecules on graphene, and show that the experimental data can only be described by a sticking probability that is exponentially decaying with increasing NO_2 coverage. We present the resulting model for the adsorption of NO_2 molecules on graphene, and relate the number of adsorbed molecules to the measured sensor response.

We assume that the NO_2 molecules remain intact upon adsorption, and denote the total number of available binding sites on the graphene surface as N_S, and the total number of bound NO_2 molecules as N. We set the time $t = 0$ to the instant where the NO_2 is added into the gas flow. Note that at $t = 0$ the surface is not completely free from NO_2 molecules, since there will be those bound to very strong binding sites. We consider these sites as inert, and assume that these NO_2 molecules will remain bound to these sites throughout, so that they are not part of the N_S available binding sites, and we do not include them in the total number of bound NO_2 molecules N. The adsorption rate is then proportional to the density of NO_2 molecules in the gas phase, n_G, times the number of free adsorption sites, $N_S - N$. We denote the proportionality factor as the sticking probability, k_A, and it includes the probability of a gas phase molecule hitting the graphene surface in a given time-interval, and all the subsequent physical processes that NO_2 undergoes upon adsorption, which can be described with their effective adsorption barrier, E_A, so that $k_A \propto e^{-E_A/k_BT}$. Here k_B is the Boltzmann constant and T is the temperature. The desorption rate is proportional to the number of adsorbed NO_2 molecules, and we denote the proportionality factor as the desorption coefficient, k_D, which includes all physical processes that NO_2 undergoes upon desorption, and which are described by the energy barrier E_D, so that $k_\mathrm{D} \propto e^{-E_D/k_BT}$. For a pristine graphene surface E_A is approximately zero, and E_D is equal to the binding energy, E_B. In the experiments considered here the graphene surface is exposed to ambient air also before the NO_2 is added, so that part of the surface is covered with ambient molecules such as N_2 and O_2. The activation energy then corresponds to the energy barrier for replacement of these ambient molecules by NO_2.

The total rate of change of NO_2 molecules on the graphene surface can then be written as a Langmuir type differential equation

$$\frac{dN}{dt} = n_G k_A \left(N_S - N\right) - k_D N, \tag{S2}$$

where t is the time. We can now introduce the relative change in the number of adsorbed NO_2 molecules, $n = N/N_S$ $(0 \leq n \leq 1)$, which allows us to rewrite equation (S2) as

$$\frac{dn}{dt} = n_G k_A \left(1 - n\right) - k_D n. \tag{S3}$$

The experimentally measured sensor response, S, is given by the relative difference between the time-dependent linewidth, $\omega(t)$, and the linewidth at time 0, ω_0

$$S(t) = \frac{\omega(t) - \omega_0}{\omega_0}. \tag{S4}$$

We now assume that $S(t) = n(t)$, so that a change in relative NO_2 coverage leads to an equal change in the sensor response, and we can rewrite equation (S6) directly in terms of sensor response as

$$\frac{dS}{dt} = n_G k_{\mathrm{A,S}} \left(1 - S\right) - k_{\mathrm{D,S}} S, \tag{S5}$$

where the additional subscripts "S" in $k_{\mathrm{A,S}}$ and $k_{\mathrm{D,S}}$ indicate that these are effective coefficients for the changes in the sensor response, which are not necessarily equal to the ones for the change

in n. We will consider the general case $S(t) = c(n(t))\ n(t)$, with an arbitrary monotonic function $c(n)$, at the end of this section. Equation (S5) can be solved analytically to give

$$S(t) = n(t) = S_\infty \left(1 - e^{-(n_G k_{\mathrm{A,S}} + k_{\mathrm{D,S}})t}\right), \qquad \text{with} \quad S_\infty = \frac{n_G k_{\mathrm{A,S}}}{n_G k_{\mathrm{A,S}} + k_{\mathrm{D,S}}}. \tag{S6}$$

We can now obtain estimates for the parameters $k_{\mathrm{A,S}}$ and $k_{\mathrm{D,S}}$ by fitting this equation to the experimental data. In all our calculations we fit the theoretical models to the data at the lowest, $n_G = 0.3$ ppm, and highest, $n_G = 100$ ppm, NO_2 gas phase concentrations. We denote these data sets as our training data sets. We then use the experimental data at the remaining concentrations to test the quality of the fit. The resulting values for $k_{\mathrm{A,S}}$ and $k_{\mathrm{D,S}}$ are given in Figure S9a, and in Figure S9f where the model data is compared to the experiment. The agreement between model and experiment is not good, which indicates that the use of constant $k_{\mathrm{A,S}}$ and $k_{\mathrm{D,S}}$ is not a realistic assumption.

S7.1 Position dependent adsorption and desorption coefficients

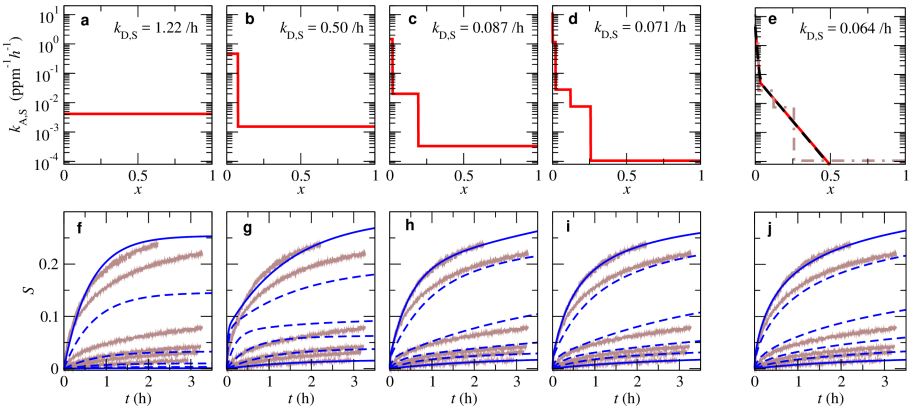

Figure S9: (a-e) The effective rate of adsorption $k_{\mathrm{A,S}}/\gamma_D$ as a function of effective surface position, x, and the resultant theoretical sensor responses (f-j). The theoretical fittings (blue curves) are superimposed on top of the experimental data (brown curves). The theoretical parameters are obtained by fitting the theoretical model to the 0.3 and 100 ppm NO_2 data (solid blue curves). The dashed blue curves are the theoretical sensor response for the other NO_2 gas phase concentrations, not used for the fitting, which therefore correspond to the test set for the validity of the model. The step-wise curves in (a-d) are calculated with equation (S9) (1 step for a, 2 for b, 3 for c, and 5 for d), the continuous red curve in e is calculated with equation (S13), and the black dash curve with equation (S15). The dash-dotted brown curve in 3 is a copy of the curve in d, and shows that the continuous functions smoothly average the step-wise functions.

To better describe experiment we can subdivide the total number of active sites on the graphene into i_{max} smaller subsets, $N_{S,i}$, so that $\sum_{i=1}^{i_{max}} N_{S,i} = N_S$. The relative weight of each subset, w_i, is defined as $w_i = N_{S,i}/N_S$, so that $\sum_{i=1}^{i_{max}} w_i = 1$. We can then generalize equation (S5) as

$$\frac{dS}{dt} = \sum_{i=1}^{i_{max}} w_i \left[n_G k_{\mathrm{A,S},i} \left(1 - S_i\right) - k_{\mathrm{D,S},i} S_i\right], \qquad \text{with} \quad S = \sum_{i=1}^{i_{max}} w_i S_i, \tag{S7}$$

and where $k_{\mathrm{A,S},i}$ ($k_{\mathrm{D,S},i}$) is the sticking (desorption) coefficient for the subset with index i. In this way we describe the graphene surface as having i distinct regions with different properties,

so that each has its own adsorption and desorption coefficient. The analytic solution for each $S_i(t) = n_i(t)$ has analogous form to the one given in equation (S6). When comparing the model to the experiment we find that subdividing k_D in smaller subsets does not significantly improve the agreement with experiment, so that in what follows we therefore use a constant value for k_D. We will discuss this in more detail further down in this section, in general this shows that the adsorption process is dominated by variations in the sticking rate rather than the desorption rate.

Without loss of generality we can order the subsets in such a way that $k_{\mathrm{A,S},i+1} \leq k_{\mathrm{A,S},i}$. We now introduce the variable $x \in [0,1]$, and write the sticking rate as function of this variable as

$$k_{\mathrm{A,S}}(x) = \begin{cases} k_{\mathrm{A,S},1} & 0 \leq x < w_1 \\ k_{\mathrm{A,S},2} & w_1 \leq x < w_1 + w_2 \\ k_{\mathrm{A,S},3} & w_1 + w_2 \leq x < w_1 + w_2 + w_3 \\ \vdots & \\ k_{\mathrm{A,S},i_{max}} & 1 - w_{i_{max}} \leq x \leq 1 \end{cases}, \tag{S8}$$

or in a more compact notation

$$k_{\mathrm{A,S}}(x) = \sum_{i=1}^{i_{max}} k_{\mathrm{A,S},i} \left[\theta(x - x_i) - \theta(x - x_i - w_i)\right] \quad \text{, with} \quad x_i = \sum_{j=1}^{i-1} w_j, \tag{S9}$$

where $\theta(x)$ is the Heaviside step function. This corresponds to a step-wise monotonically decreasing function, where the value at each step is equal to a given $k_{\mathrm{A,S},i}$, and the width of the step is equal to w_i. We interpret x as an effective variable describing different positions of the graphene surface, and write the position dependent occupation probability in analogous form as

$$S_x(x) = n_x(x) = \sum_{i=1}^{i_{max}} S_i \left[\theta(x - x_i) - \theta(x - x_i - w_i)\right] \quad \text{, with} \quad x_i = \sum_{j=1}^{i-1} w_j. \tag{S10}$$

This allows us to write equation (S7) in an equivalent integral form as

$$\frac{dS}{dt} = \frac{dn}{dt} = \int_0^1 \left[n_G k_{\mathrm{A,S}}(x)\left(1 - S_x(x)\right) - k_{\mathrm{D,S}} S_x(x)\right] dx, \qquad \text{with} \quad S = \int_0^1 S_x(x) dx, \tag{S11}$$

which has the analytic solution

$$S(t) = n(t) = \int_0^1 S_\infty(x) \left(1 - e^{-(n_G k_{\mathrm{A,S}}(x) + k_{\mathrm{D,S}})t}\right) dx, \qquad \text{with} \quad S_\infty(x) = \frac{n_G k_{\mathrm{A,S}}(x)}{n_G k_{\mathrm{A,S}}(x) + k_{\mathrm{D,S}}}. \tag{S12}$$

Instead of a sum over discrete values $S(t)$ is expressed as an integral over the effective position variable x. The advantage is that this integral form is valid for any arbitrary $k_{\mathrm{A,S}}(x)$, not only for the stepwise decaying function discussed so far.

We start by presenting results for $i_{max} = 2$ in Figure S9bg, and find that $k_{\mathrm{A,S},1}$ is about two orders of magnitude larger than $k_{\mathrm{A,S},2}$, and that the weight of the first region is much smaller than the one of the second region. While the agreement with experiment is improved compared to using only one region, it is still rather poor. This shows that while for each individual value of n_G one can fit the experimental data well with two exponentials, since the fitting parameters for a each n_G are independent of the ones at a different n_G, to have a physically consistent model across varying n_G (equation (S12)) two exponentials are not enough. The agreement between theory and experiment becomes reasonable for $i_{max} = 3$ (S9ch), and becomes eventually rather good for $i_{max} = 5$ (S9di). Also in these cases the values of the $k_{\mathrm{A,S},i}$ decrease on an exponential scale as x is

increases, and the weights become progressively larger as $k_{\mathrm{A,S},i}$ decrease. For small x the function $k_{\mathrm{A,S}}(x)$ therefore exhibits exponentially decreasing behavior. For large x the value of $k_{\mathrm{A,S}}(x)$ is very small, so that the model function does not significantly change when replacing the value with zero.

Having determined that the general $k_{\mathrm{A,S}}(x)$ needs to be an exponentially decaying function, we can replace the step functions with continuous exponential functions with piecewise linear variation of the exponents as

$$k_{\mathrm{A,S}}(x) = k_{\mathrm{A,S},0}\ e^{\sum_{i=1}^{i_{max}}[f_i-\alpha_i(x-x_i)][\theta(x-x_i)-\theta(x-x_i-w_i)]}\,[\theta(x)-\theta(x-1)]\,, \tag{S13}$$

with

$$x_i = \sum_{j=1}^{i-1} w_j, \quad \text{and} \quad \alpha_i = \frac{f_i - f_{i+1}}{w_i}, \tag{S14}$$

where $f_1 = 1$, and $k_{\mathrm{A,S},0}$, f_i, and w_i are arbitrary parameters. Note that this function is zero outside the range $x \in [0, 1]$. We then obtain $n(t)$ by numerically evaluating equation (S12). While this function is now continuous, it still has discontinuous derivatives. An alternative exponentially decreasing function with continuous derivatives can be obtained adding up exponential terms with different exponents, which gives the simpler form

$$k_{\mathrm{A,S}}(x) = \sum_{i=1}^{i_{max}} k_{\mathrm{A,S},i}\ e^{-\alpha_i x}, \tag{S15}$$

where now both $k_{\mathrm{A,S},i}$ and α_i are parameters.

When fitting equation (S13) or equation (S15) to experiment for $i_{max} = 1$ the agreement is not very good. For $i_{max} = 2$ on the other hand the agreement is already excellent (Figure S9ej). The required number of parameters for the exponentially decreasing continuous $k_{A,x}(x)$, 5 for $i_{\max} = 2$, is therefore much smaller then the one required for a good agreement with experiment for the stepwise function considered earlier, where $i_{\max} \geq 5$ is required (Figure S9). This further confirms that the exponentially decaying functional form is a good representation of the underlying physical processes. We note that the fitted $k_{A,x}(x)$ is essentially identical using either equation (S13) or equation (S15) (Figure S9e), except that when using equation (S13) there is a kink in the function, while with equation (S15) the function is smooth everywhere, so that in general we choose this functional form. For $n_G = \{0.3, 1.0, 100.0\}$ ppm the agreement is essentially perfect. For $n_G = \{3.0, 10.0, 50.0\}$ the agreement is still good, and can be brought into perfect overlap with experiment when rescaling the function by a constant, or evaluating it at a slightly shifted n_G. We attribute this to slightly varying experimental conditions across the experimental runs for different n_G, as also discussed further down in Figure S10. For example, one can see that the experimental curves for 1 and 3 ppm are very close to each other, while one would expect the spacing to be more similar to the one between 0.3 and 1 ppm. Indeed the model predicts such a larger spacing. For larger i_{max} the agreement with experiment does not improve significantly, which shows that the true shape of $k_A(x)$ is well captured with two exponentials.

Since as discussed at the beginning of this section $k_A \propto e^{-E_A/k_BT}$, we propose that the physical origin of the observed variation in the exponent of equation (S13) is mainly determined by the variation of E_A across the surface. The good agreement of equation (S13) with experiment for $i_{max} = 2$ shows that this variation is approximately piece-wise linear with two different slopes. In general the adsorbed NO_2 molecules interact with each other, for example due to electrostatic repulsion of these negatively charged molecules, so that the activation barrier is expected to increase with increasing coverage, even for a perfectly homogeneous graphene surface. Moreover, the charge transfer per NO_2 molecule will generally decrease for increasing coverage due to electrostatic interactions, and the change in mobility for a given adsorbed molecule can also vary with

coverage. The extracted $k_{\mathrm{A,S}}(x)$ in Figure S9e therefore is a universal unction, which includes the variation of the activation barrier due to an inhomogeneous surface, and implicitly also due to the inter-molecular interactions, as well as the changes of charge transfer and mobility with coverage.

S7.2 Coverage dependent adsorption and desorption coefficients

As an alternative/equivalent way, instead of expanding the sticking coefficient as a function position, x, we can also expand it as function of surface coverage, n, or equivalently of S, since we assume that $S = n$. The variations of the sticking coefficient with $S = n$ includes both the effects due to molecule-molecule interactions, but also implicitly the graphene surface inhomogeneities. In analogy to equation (S15) we can write this dependence as a sum of exponentially decaying functions

$$k_{\mathrm{A,S}}(S) = \sum_{i=1}^{i_{max}} \bar{k}_{\mathrm{A,S},i}\; e^{-\bar{\alpha}_i S}, \tag{S16}$$

with parameters $\bar{k}_{\mathrm{A,S},i}$ and $\bar{\alpha}_i$.

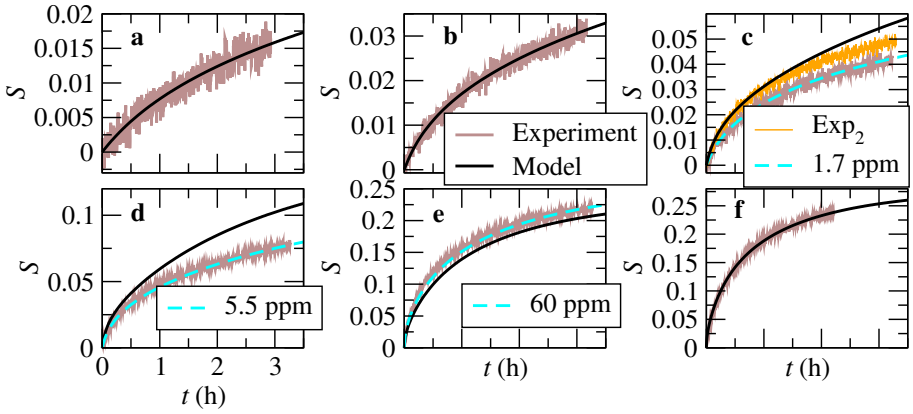

Figure S10: Time dependent sensor response for all the measured NO_2 concentrations: (a) 0.3 ppm, (b) 1 ppm, (c) 3 ppm, (d) 10 ppm, (e) 50 ppm, and (f) 100 ppm. Brown curves are the experimental data, black curves the theoretical results, obtained using equation (S17) for constant $k_{\mathrm{D,S}}$. The fitted $k_{\mathrm{A/D,S}}(S)$ are shown as green dashed curves in Figure S11. The agreement between theory and experiment is rather good for all curves. For the fitting sets (0.3 ppm and 100ppm, also denoted as training sets) the agreement is essentially perfect, and also for the test set in (b). For the test sets in (c-e) there are some quantitative deviations between experiment and theory. Theory and experiment can be brought to essentially perfect overlap also for these cases if the calculations are performed for concentrations that slightly differ from the nominal experimental values (dashed cyan curves). We therefore attribute the quantitative deviations in the test sets to slightly different experimental conditions for each measurement run. For example, the orange curves in (c) are for a second experimental run at 3 ppm, and these are significantly closer to the theoretical model, indicating the range of variability in the experimental measurements.

We then obtain $S(t)$ by numerically solving the differential equation

$$\frac{\partial}{dt} = n_G\; k_{A,S}(S)\,(1-S) - k_{D,S}(S)\; S. \tag{S17}$$

Here we have also added the possibility of having a coverage dependent desorption coefficient, $k_{D,S}(S)$. This equation corresponds to equation (S5), generalized to include $S-$dependent sticking

and desorption coefficients. We first present results for a constant $k_{\mathrm{D,S}}$. As found for the x-dependent case, also here for $i_{max} = 2$ the theoretical model agrees well with experiment (Figure S10 and Figure 3d in the main manuscript). The resulting $k_{\mathrm{A/D,S}}$ are shown in Figure S11. The quality of the fit is essentially identical to the one for position, x, dependent $k_{\mathrm{A/D,S}}$, showing that the two models capture the same physical processes.

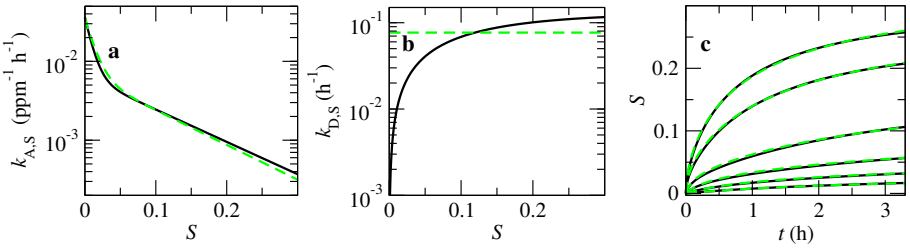

Figure S11: (a) Effective sticking coefficient as function of sensor response (equation (S16)), S, and (b) effective desorption coefficient as function of S (equation (S18)), as well as (c) the resulting S as function of time (equation (S17)). The green dashed curves are for a constant desorption coefficient, while the black solid curves are for the monotonically increasing desorption coefficient. As can be seen in (c) both models for the desorption coefficient give essentially identical theoretical sensor response, showing that $S(t)$ is mainly determined by the adsorption coefficient. Good agreement is also found when comparing to experiment, as shown in Figure S10.

We now demonstrate that the results are rather insensitive to the functional form of $k_{D,S}(S)$ by comparing the results so far with the ones obtained with a non-constant $k_{D,S}(S)$. Here we use a monotonically increasing function, since in general it can be expected that the desorption coefficient increases with increasing NO_2 coverage. As an example we choose the following form for the desorption coefficient

$$k_{D,S}(S) = k_{\mathrm{D,S},0} + \sum_{i=1}^{i_{\mathrm{D,max}}} k_{\mathrm{D,S},i} \left(1 - e^{-\beta_i S}\right), \tag{S18}$$

with fitting parameters $k_{\mathrm{D,S},0}$, $k_{\mathrm{D,S},i}$, and β_i. For $i_{max} = 2$ and $i_{\mathrm{D,max}} = 1$ the results fitted to experiment shown in Figure S11, and compared to the ones with constant $k_{\mathrm{D,S}}(S)$. As can be seen, the fitted non-constant $k_{D,S}(S)$ is approximately 0 for small S, and rises for increasing S, and is therefore significantly different from the constant k_D. Nevertheless, $k_{A,S}(S)$ is almost unchanged when compared to the case of constant k_D, showing that obtained functional form of $k_{A,S}(S)$ is robust, and largely independent on the shape of $k_{D,S}(S)$. In Figure S11c it can be seen that the model gives essentially identical results for both constant $k_{D,S}$ and non-constant $k_{D,S}(S)$, and the agreement with experiment is only marginally improved. These results show that for the available experimental data we cannot extract the detailed shape of $k_{D,S}(S)$, while they allow us to reliably obtain $k_{A,S}(S)$, which determines the adsorption process in these experiments. Using a constant $k_{\mathrm{D,S}}$ we obtain an approximate average value for the large coverage regime. For small coverage the true $k_{D,S}(S)$ can be smaller than this value, but not larger.

We conclude this section by discussing the effect of varying the arbitrary monotonic function $c(n)$, which relates the sensor response to the NO_2 surface coverage,

$$S(t) = c(n_c(t))\; n_c(t), \tag{S19}$$

where the subscript "c" explicitly denotes that the dependence of the NO_2 surface coverage on the function $c(n)$. A non-constant $c(n)$ can be caused for example by the fact that the charge

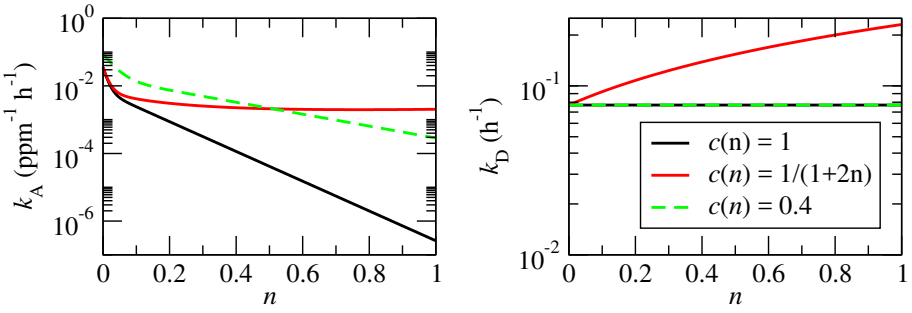

Figure S12: Molecular sticking, k_{A}, and desorption, k_{D}, coefficients calculated with Eqs. (S25,S26), using $k_{\mathrm{A},S}$ and $k_{\mathrm{D},S}$ fitted to experiment for constant $k_{\mathrm{D,S}}$ (Figure S11a,b, green dashed curves), for different functional forms of $c(n)$.

transfer per NO_2 molecule to graphene is reduced as more NO_2 molecules are adsorbed due to the electrostatic repulsion between the transferred electrons. Since in the experiments considered here the graphene surface is already p-doped at $t = 0$, we expect that this variation is rather small and continuous. The possible range of $c(n)$ is limited by physical constraints. Its lowest possible value set by the largest measured sensor response, $S_{\max} = c(n_{\max})n_{\max} \leq c(n_{\max})$. The experimentally measured maximum sensor response is about 0.26, so that in our case we have $c(n) \geq 0.26$. Since $S(t)$ appears to still be rising at the largest measured times, we can expect the minimal $c(n)$ to be somewhat larger. Furthermore, we expect the maximum $c(n)$ to be of the order of about one, in which case a given change in the surface coverage leads to an equal change in the sensor response.

We will now show that $n_c(t)$ can be obtained from $n_1(t)$, where the subscript "1" indicates that it is obtained for $c(n) = 1$, as calculated in the previous part of this section. To reproduce the same signal for both cases the condition

$$S = n_1 = c(n_c)n_c \tag{S20}$$

needs to be satisfied. With this relation we first rewrite the differential equation (S17) as

$$\frac{dn_1}{dt} = \frac{dS}{dt} = n_G \; k_{A,S}(S)\,(1 - S) - k_{D,S}(S) \; S. \tag{S21}$$

Using the relation $n_1 = c(n_c)n_c$ this equation can be written in terms of n_c as

$$\frac{dn_c}{dt} = n_G \; \frac{1}{g(n_c)} \; \frac{1}{c(n_c)} k_{A,S}(c(n_c) \; n_c)\,(1 - c(n_c)n_c) - \frac{1}{g(n_c)} k_{D,S}(c(n_c)n_c) \; n_c, \tag{S22}$$

with

$$g(n) = 1 + n\frac{d\ln\left[c(n)\right]}{dn}. \tag{S23}$$

If we assume that $n_c \ll 1$, we can approximate the term $(1 - c(n_c)n_c) \approx 1 \approx (1 - n_c)$. We can then approximate equation (S22) as

$$\frac{dn_c}{dt} = n_G \; k_A(n_c)\,(1 - n_c) - k_D(n_c)n_c, \tag{S24}$$

with

$$k_A(n) \approx \frac{1}{g(n)} \; \frac{1}{c(n)} k_{A,S}(c(n) \; n) \tag{S25}$$

$$k_D(n) \approx \frac{1}{g(n)} \; k_{D,S}(c(n) \; n). \tag{S26}$$

For a given $S(t)$ we therefore first evaluate the functional form of the universal functions $k_{A,S}(S)$ and of $k_{D,S}(S)$, and can then use Eqs. (S25,S26) to obtain adsorption and desorption coefficients for any arbitrary $c(n)$, and with them the NO_2 surface coverage by numerically solving equation (S24) with these coefficients.

To illustrate the process we present k_A and k_D, evaluated using Eqs. (S25, S26), for three representative choices for $c(n)$ (Figure S12): $c(n) = 1$, $c(n) = 1/(1 + 2n)$, and $c(n) = 0.4$. For $k_{A,S}$ and $k_{D,S}$ we use the previously obtained results for constant $k_{D,S}$, shown as green dashed lines in Figure S12. The first choice of $c(n)$ corresponds to a constant and rather large value of c, while the third one corresponds to a small constant value close to the lowest possible limit. It can be seen that k_D is identical for both cases, and that for the smaller $c(n) = 0.4$ the value of k_A is larger than for $c(n) = 1$. This corresponds to the expected behavior, since for a smaller $c(n)$ more NO_2 molecules are needed to produce the same sensor response obtained for larger $c(n)$. The second chosen functional form, $c(n) = 1/(1+2n)$, corresponds to a $c(n)$ decreasing with increasing n. This is the generally expected behavior, since for increasing charge transfer between NO_2 molecules and graphene the electrostatic repulsion between electrons in the graphene sheet makes it increasingly difficult to further increase the charge inside the graphene, and therefore the rise of the sensor response is reduced. In this case both k_A and k_D are changed compared to $c(n) = 1$, with k_D increasing with increasing n. The decay of k_A with increasing n is reduced compared to the $c(n) = 1$ case, since progressively more adsorbed NO_2 molecules are needed to produce the same sensor response.

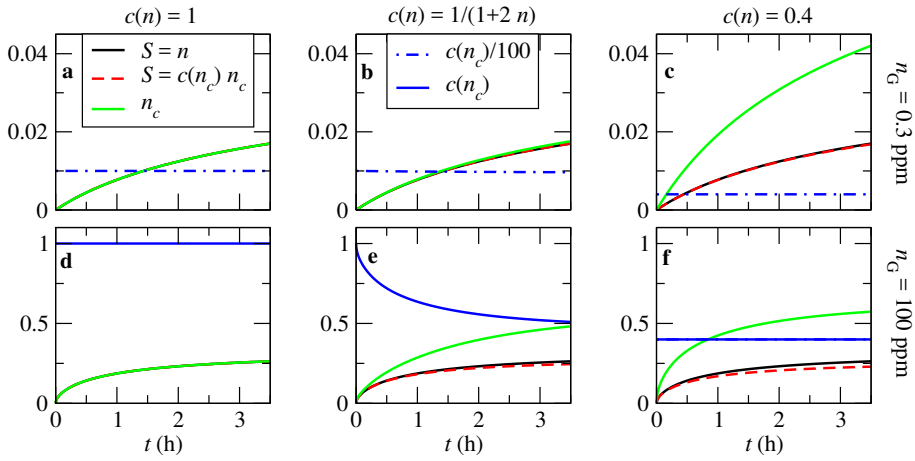

Figure S13: Sensor response for $S = n$ (solid black curves) and for $S = c(n_c)n_c$ (red dashed curves), as well as NO_2 surface occupation n_c (green curves), and $c(n_c)$ (blue curves) as function of time, for various NO_2 gas phase concentrations, n_G [(a-c) $n_G = 0.3$ ppm, (d-f) $n_G = 100$ ppm], and functional forms of $c(n)$ [(a,d) $c(n) = 1$, (b,e) $c(n) = 1/(1 + 2n)$, (c,f) $c(n) = 0.4$]. The corresponding k_A and k_D are shown in Figure S12. Note that to have all plots on a similar scale in the upper panels we show the values of $c(n_c)$ divided by hundred (dot-dashed blue curves).

To evaluate the validity of Eqs. (S25,S26) for such systems we calcualte $S(t)$ both from $k_{A/D,S}$, as well as using $k_{A/D,n}$ from these equations, which we denote as $S_c(t)$. As can be seen in Figure S13 $S(t)$ and $S_c(t)$ are either identical or very close to each other for all considered cases, which confirms the validity of the equations. In Figure S13 one can also see that the smaller $c(n)$, the larger n compared to S, showing that more NO_2 molecules need to be adsorbed to produce the same sensor response.

We conclude by noting that we can also invert equation (S20) and express n_c as function of S,

$n_c = S/\tilde{c}(S)$, and then write these quantities in terms of sensor response as

$$k_{A,S}(S) \approx g(\frac{S}{\tilde{c}(S)})\ \tilde{c}(S)\ k_A(\frac{S}{\tilde{c}(S)}) \tag{S27}$$

$$k_{D,S}(S) \approx g(\frac{S}{\tilde{c}(S)})\ k_D(\frac{S}{\tilde{c}(S)}). \tag{S28}$$

This explicitly shows that the effective sticking and desorption coefficients, $k_{A,S}(S)$ and $k_{D,S}(S)$, include both the effects of the molecular sticking and desorption coefficients, k_A and k_D, as well as of the sensor response as function of molecular coverage, $\tilde{c}(S)$. Using these effective sticking coefficients, $k_{A,S}(S)$ and $k_{D,S}(S)$, it is therefore possible to describe the experimental sensor response without explicit knowledge of $c(n)$.

References

[1] Hao L, Gallop J, Liu Q and Chen J 2015 *IET Circuits, Devices & Systems* **9** 397–402

[2] Shautsova V, Gilbertson A M, Black N C G, Maier S A and Cohen L F 2016 *Scientific Reports* **6** 30210

[3] Suk J W, Kitt A, Magnuson C W, Hao Y, Ahmed S, An J, Swan A K, Goldberg B B and Ruoff R S 2011 *ACS Nano* **5** 6916–6924 URL http://dx.doi.org/10.1021/nn201207c

[4] Li X, Zhu Y, Cai W, Borysiak M, Han B, Chen D, Piner R D, Colombo L and Ruoff R S 2009 *Nano Letters* **9** 4359–4363 URL http://dx.doi.org/10.1021/nl902623y

[5] Liang X, Sperling B A, Calizo I, Cheng G, Hacker C A, Zhang Q, Obeng Y, Yan K, Peng H, Li Q, Zhu X, Yuan H, Hight Walker A R, Liu Z, Peng L m and Richter C A 2011 *ACS Nano* **5** 9144–9153 URL http://dx.doi.org/10.1021/nn203377t

[6] Her M, Beams R and Novotny L 2013 *Physics Letters A* **377** 1455–1458 ISSN 0375-9601 URL http://www.sciencedirect.com/science/article/pii/S0375960113003617

[7] Ziegler D, Gava P, Güttinger J, Molitor F, Wirtz L, Lazzeri M, Saitta A M, Stemmer A, Mauri F and Stampfer C 2011 *Phys. Rev. B* **83** 235434 URL http://link.aps.org/doi/10.1103/PhysRevB.83.235434